Ashish Pathak, et. al. International Journal of Engineering Research and Applications
www.ijera.com
ISSN: 2248-9622, Vol. 16, Issue 8, August 2026, pp 19-27

RESEARCH ARTICLE OPEN ACCESS

Coupled Thermomechanical FE Analysis for Distortion and Residual Stress Prediction in Seam Welding of Thin Pipe

Ashish Pathak[1] Sachin Kumar Nikam[2], Chandra Pal Singh[3], Gajendra Kumar Nhaichaniya[4], Anshul Kumar Bansal[5]

[1] Research Scholar, Mechanical Engineering Department, LNCT University Bhopal, M.P., India
[2] Associate Professor, School of Computer, Science & Technology, LNCT University Bhopal, M.P., India
[3] Assistant Professor, Mechanical Engineering Department, SATI (Engg. College), Vidisha M.P., India
[4]Assistant Professor, Department of Mechanical Engineering, FET, Poornima University Jaipur
[5]Assistant Professor, Mechanical Engineering Department, RTU Kota, Rajasthan, India
Corresponding Author: Chandra Pal Singh

Abstract
This research aims to numerically investigate seam welding in 304 stainless steel pipes. A fully coupled transient thermo-mechanical simulation technique is employed to replicate welding behavior on a single-pass cylindrical seam joint with a nominal diameter of 80mm and a thickness of 1.5mm. The Goldak heat source model is employed to represent the moving welding heat source. The maximum temperature reached 1773K in the Heat-Affected Zone (HAZ), while away from the HAZ, it is below 350 K. Due to this temperature gradient, high thermal stresses are generated, and even after cooling, residual stresses of order 177 MPa are observed. However, the residual stresses are lower than the material's yield stress. The average value of distortion in the weld seam is 2.1 mm, while the maximum distortion of 2.5 mm occurs at the end.Based on the findings from the Finite Element (FE) Analysis, decisions can be made regarding changes to the welding method or adjustments to parameters if deemed necessary.
Keywords – TIG welding, pipe seam welding, transient thermo-mechanical FE analysis

Date of Submission: 05-08-2026 Date of acceptance: 19-08-2026

I. Introduction

Seam welding is a critical manufacturing process due to the involvement of critical weld and process parameters[1], [2], [3], [4], [5]. This welding causes localized heating and quick cooling in thin pipes, which concentrates weld residual stresses along the weld bead [4], [5].The mechanical qualities of these joints, such as brittle fracture, resistance and fatigue performance, might be negatively impacted by produced residual stresses[6]This welding method is widely used in the fabrication of thin-walled pipes for applications in the food and pharmaceutical industries, power plants, and the automotive and aerospace industries[7], [8], [9]. In the above-mentioned applications, Welding joints are often required to meet dimensional accuracy, structural integrity, corrosion resistance, and fatigue life. The Austinic stainless steel AISI 304 is widely acceptable for dear excellent corrosion resistance, good formability and favorable mechanical properties[10], [11], [12]. However, despite these advantages, welding thin-walled stainless steel pipes presents significant challenges due to their high thermal sensitivity and constrained geometries.

In the pipe industry, thin pipes have a low thickness-to-diameter ratio; they are therefore very sensitive to welding due to their low thickness [13], [14]. The localized transient heat during the seam weld leads steep temperature gradient, especially in the welded zone [15]. Hence, non-uniform thermal expansion and contraction lead to significant distortion and residual stresses in the final component. Even a small distortion can render the component unusable due to misalignment during assembly, while residual stress can make it prone to fatigue failure. For these reasons, controlling distortion and residual stress is paramount in thin Pipe welding [16], [17]. However, achieving optimal welding parameters based on experimental try and error is very costly and time-consuming and many times it is impractical. Especially when various welding parameters, machine parameters and temperature-dependent material properties are included in the process.

FE-based numerical simulations emerged as a powerful and reliable tool for predicting the welding-induced thermal and mechanical behaviour under various machine and material conditions [18]. In waddling simulation, coupled transient thermo-mechanical analysis has gained attention as it simultaneously enables the temperature and structural coupling during the welding process. With this simulation technique, thermal strain, residual, and distortion patterns can be evaluated even before physically welding the components [19]. Unlike the uncoupled or sequential approach, the fully coupled thermo-mechanical simulation captures the interaction between thermal and mechanical fields during the welding process, which is especially important for thin structures where the mechanical response is highly sensitive to the thermal loading.

Seam welding presents unique challenges due to moving heat, cylindrical geometry, and small wall thicknesses that locally melt and solidify rapidly [20], [21]. To consider the weld pool effect during the welding process double-ellipsoidal Goldak heat-source model is widely acceptable as it represents realistic weld-pool shapes and heat distribution [22], [23]. The appropriate Goldak heat source parameters can be determined using experiments and an ANN-based prediction[24]. With appropriately calibrated Goldak model parameters, it is possible to closely replicate experimental weld-bead geometry and thermal histories using numerical welding simulations.

The residual stresses generated in seam welding are primarily due to the non-uniform thermal cycle experienced by the Weld metal in the HAZ. During heating, the material undergoes thermal expansion, but this is constrained by the surrounding low-temperature material, resulting in high compressive stresses. Upon cooling, contraction of the weld material is restrained, resulting in tensile residual stress in the pipe that may exceed the material's yield strength. Further, in thin pipes, these residual stresses are often highly non-uniform along thickness and circumferential direction so the prediction becomes more challenging [25], [26].In stainless steels, tensile residual stresses at the inner surface of pipes are known to increase susceptibility to stress corrosion cracking[27], [28]. Therefore, a detailed understanding of residual stress distribution induced by seam welding is critical for ensuring safe and reliable operation.In addition to residual stresses, welding-induced distortion is a major concern in the fabrication of thin-walled pipes[29], [30], [31].

In this research, a fully coupled transient thermomechanical FE approach is used to investigate seam welding in thin-walled stainless steel pipes. The temperature-dependent material parameters are adopted from Deng et. al[32]The moving heat sourceis formulated using the Goldak model, and appropriate boundary conditions are used to simulate the actual welding process. The seam welding of a thin-walled pipe with a nominal diameter of 80 mm and a wall thickness of 1.5 mm is considered in this study.By coupling thermal and mechanical responses, the study aims to capture temperature fields, stress distributions, final residual stresses, and distortion patterns.In addition, the study provides detailed numerical insight into the thermomechanical behaviour of thin pipes during seam welding.

1. Welding simulation workflow

Inthe welding process, machine parameters such as voltage, current, and weld speed are common variables that affect weld joint strength,distortion and residual stresses. The machine parameters are obtained from the literature[33]. The voltage is 12 volts, the current is 85 amps, while the weld speed is 150 mm/min. By adopting these established process parameters, this study primarily focused on investigatingresidual stress, distortion and temperature profile during welding. The geometry of the pipe for seam welding is depicted in Figure 1.

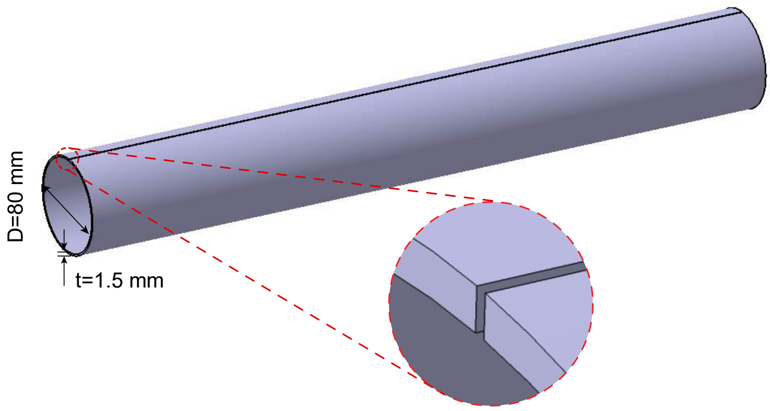

Figure 1 The weld pipe geometry

The overall workflow adopted FE analysis for seam welding, as illustrated in Figure 2. The analysis begins with the setup of the FE model for welding simulation, including the geometric modelling of the thin-walled pipe. A fine mesh is generated in the HAZ, while a coarse mesh is used outside the HAZ to reduce simulation time and mesh effort.After meshing, a quality check test is performed to ensure acceptable element quality, especially in HAZ. If the mesh does not follow the standard quality criteria, remeshing may be required.The element size in the weld zone should be small enough to capture the minimum size; here thickness is the minimum mesh size criterion. Four elements along the thickness are considered to capture the distortion behaviour accurately. The aspect ratio is below 3 while acceptable up to 5. Warpage is within 1, while the Jacobian ratio is close to 0.9.

In the next stage, material properties, loads, and boundary conditions (BCs) are assigned in the Simufact welding simulation software. Temperature-dependent thermal and mechanical properties are defined as per Table 1. The pipe is initially fixed at both ends during the welding process, while during the cooling period, it is kept free at both ends. Thermal boundary conditions account for heat losses due to convection and radiation.Subsequently, the welding heat source and robot motion are defined. A moving heat-source model is defined to represent the welding arc, along the pipe's longitudinal direction. The default Simufact solver is used to compute the time-dependent temperature distribution, thermal strains, and residual stresses throughout the welding and cooling cycles.

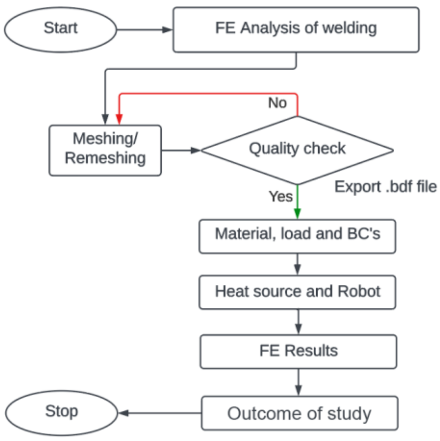

Figure 2 welding simulation workflow

2. Coupled thermo-mechanical FE analysis

Welding involves melting metals, then cooling and solidifying them to create weld beads that permanently join two parts. In finite element (FE) analysis, the welding process is treated as a coupled thermo-mechanical analysis, accounting for the effects of overall temperature on structural properties over time. To address this, Simufact offers a fully coupled transient thermo-mechanical simulation in which the temperature field is calculated at each time increment. The thermal calculation is typically less computationally demanding and scales well with the number of CPU cores. Following the thermal step, the mechanical step is executed to compute thermal strains from the temperature field and utilize them as mechanical loads for distortion and stress calculations. However, the mechanical step is generally more computationally intensive than the thermal step. Simufact welding allows defining the level of decoupling for each load case type (e.g., welding, cooling, heating), but this can increase computational expenses (not considered in this simulation study). Total run time, including welding and cooling time, to complete the simulation on 16 16-core CPU took almost 19 hours.

a) Moving heat source

The Goldak double-ellipsoid heat-source welding module is commonly used to replicate typical arc-welding processes. Introduced by Goldak et al. in 1984, this model accurately predicts heat input during welding, utilizing two ellipsoids to represent the welding arc and molten pool. It forecasts temperature distribution, phase transformation, and residual stress. It has been successfully applied to various welding techniques, including laser and friction stir welding, and has been shown to model the moving heat source accurately, addressing challenges posed by the complex interaction between the welding flame and the weld pool. Goldak proposed a three-dimensional model with a Gaussian distribution of power density in an ellipsoid welding pool, centred at coordinates (x0, y0, z0), with semi-axes a, b, and c corresponding to x, y, and z directions, respectively (seeFigure 3). The total heat input relates to applied voltage (V), current (I), and welding efficiency (η) (Eq. 1).

$$q(x,y,z) = \frac{6\sqrt{3}Q}{abc\pi\sqrt{\pi}} e^{-\frac{3(x-x_0)^2}{a^2}} e^{-\frac{3(y-y_0)^2}{b^2}} e^{-\frac{3(z-z_0)^2}{c^2}} \ldots\ldots\ldots..(1)$$

$$Q = \eta \times VI$$

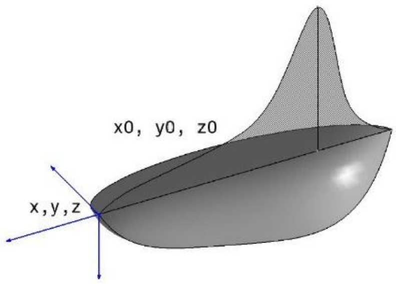

Figure 3 Goldak heat source model

b) Mesh model

The meshing of the pipe and its associated support structures, such as the bed, clamps, and joints, is performed using HyperMesh software (Figure 4). A hexahedral mesh is generated for the entire pipe geometry.A finer exahedral mesh is generated at HAZ, while a coarser mesh is generated away from HAZ. The simulation uses first-order CHEXA elements with thermal degrees of freedom. Each node of CHEXA elementoffers 3 translation degrees of freedom and one thermal degree of freedom. A single element has 24 structural and 8 thermal degrees of freedom, for a total of 32. The model comprises 33300 elements.

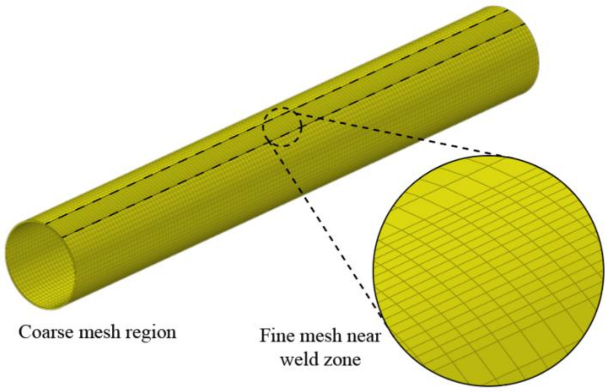

Figure 4 Pipe mesh with mesh transition technique

c) Material

The temperature-dependent material properties are crucial for such a high-temperature simulation event. At higher welding temperatures, mechanical properties change significantly, especially in the heat-affected zone (HAZ), which undergoes a thermal cycle without melting. Mechanical properties such as Young's modulus, Poisson's ratio, and yield stress are considered variable material properties with respect to temperature. At the same time, thermal properties like specific heat, conductivity, and thermal expansion are also considered temperature-dependent. Table 1 presents the selected temperature-dependent material parameters[32].

Table 1 Temperature dependent material properties.

Temp.	Density	Specific heat	Conductivity	Thermal expansion	Yield stress		Young's modulus	Possion's ratio
					Base	Weld		
(°C)	(kg/m³)	(J/kg°C)	(W/m°C)	($x10^{-5}$°C^{-1})	(MPa)	(MPa)	(Gpa)	-
0	7900	462	14.6	1.70	265	438.37	198.50	0.294
100	7880	496	15.1	1.74	218	401.96	193	0.295
200	7830	512	16.1	1.80	186	381.5	185	0.301
300	7790	525	17.9	1.86	170	361.25	176	0.310
400	7750	540	18.0	1.91	155	345.94	167	0.318
600	7660	577	20.8	1.96	149	255.71	159	0.326
800	7560	604	23.9	2.02	91	97.41	151	0.333
1200	7370	676	32.2	2.07	25	28.41	60	0.339
1300	7320	692	33.7	2.11	21	16.23	20.00	0.342
1500	7320	700	120	2.16	10	12.17	10	0.388

II. Results and Discussion

a) Temperature history

The temperature history during the welding and cooling stages of a pipe is depicted in Figure 5, which shows the temperature distribution at eight distinct time intervals: 5, 30, 60, 90, 120, 121, 150, and 1920 seconds. The welding process begins at 0 seconds and finishes after 120 seconds, while the subsequent cooling phase begins immediately after the welding stage and lasts from 120 seconds to 1800 seconds. The overall welding period is 2 minutes, with a total cooling duration of 30 minutes. The weld pool temperature exceeds the depicted peak of 1773K, reaching 5300K. However, this heightened temperature is localised within a very small zone and for a short duration.In the HAZ, the temperature reaches equilibrium between flux input and heat losses, stabilizing at an elevated temperature of 1773K. Notably, the highest temperature is localised and transient near the weld seam, ranging from 1773 to 737K, whereas the temperature in most of the pipe region remains below 350K. This temperature disparity induces significant thermal stress, causing the pipe to bend like a simply supported beam. The observed temperature difference is a primary factor contributing to the substantial thermal stress experienced by the pipe during the welding simulation.

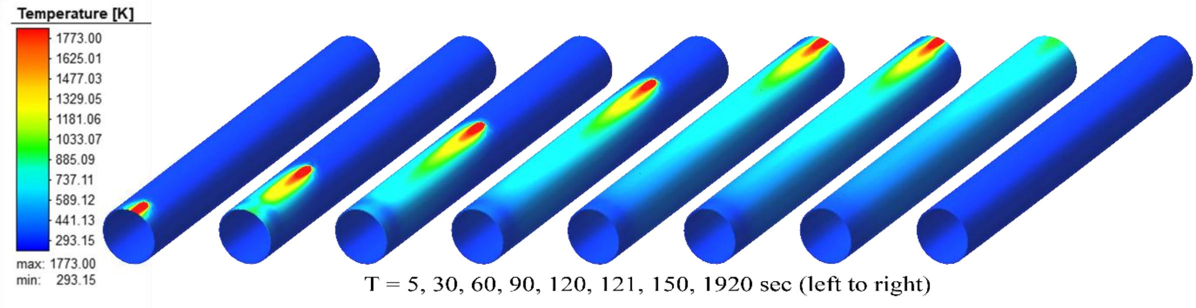

Figure 5 Temperature distribution in the pipe during welding (0-120 sec) and during cooling (120-1920 sec).

b) Stress in the pipe during seam welding

The results reveal that the welding process induces non-uniform heating along both the longitudinal and radial directions of the cylinder. As the welded region cools, differential contraction occurs, resulting in residual stresses. The distribution of these residual stresses is illustrated in theFigure 6, and the values plotted along the weld seam in Figure 7. During welding, the maximum stress is generated near clamp locations A and B (refer to the Figure 6). However, after welding,stress is released from both the A and B locations during cooling.Throughout the entire weld seam, nearly uniform stress values of approximately 177 MPa are observed, except at the clamp locations. The findings demonstrate that the provided welding inputs result in residual stresses below the yield stress. Consequently, from a failure perspective during service, the welded structure can be considered safe with respect to residual stresses.

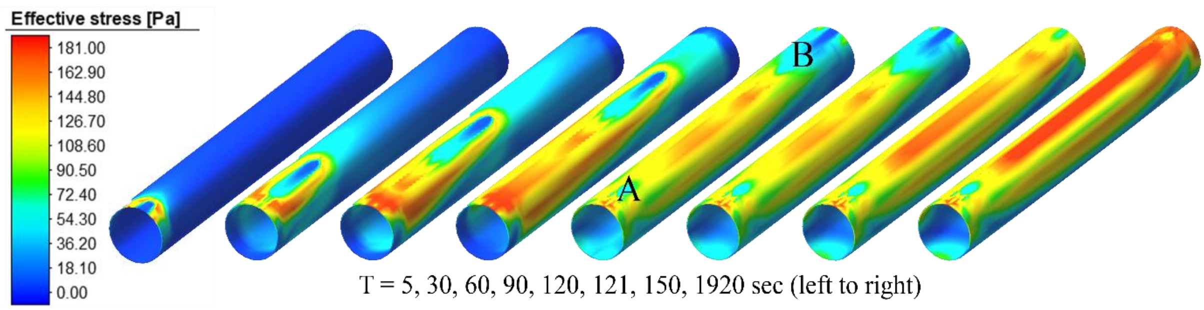

Figure 6Stress distribution in the pipe during welding (0-120 sec) and during cooling (120-1920 sec).

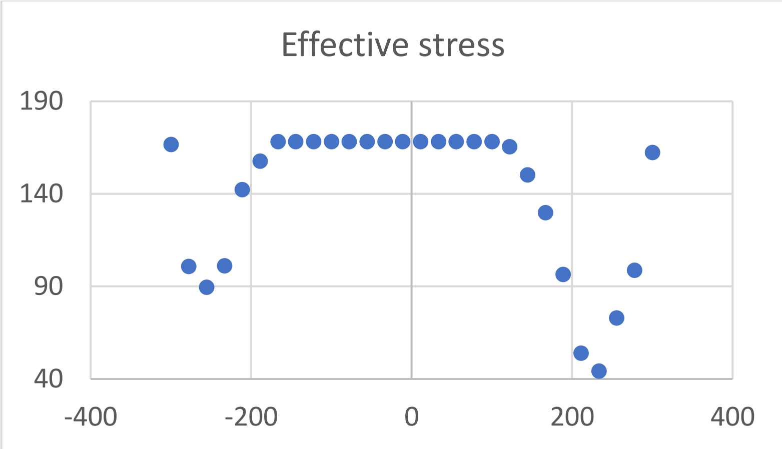

Figure 7 Stress distribution in the pipe at the end of the cooling period, after 1920 sec.

c) Distortion

An optimized combination of welding parameters has been demonstrated to yield lower distortion in pipes. The careful selection and adjustment of welding parameters, such as welding current, voltage, and travel speed, as suggested byAshish Pathak et al.[34] have shown that the distortion after welding falls within an acceptable range. During welding, the pipe is clamped, and the maximum distortion occurs near the weld pool. However, upon releasing the clamps, the distortion pattern in the pipe changes completely, and the entire pipe tends to bend like a simply supported beam. The side of the seam-weldedpipe is distorted by an average value of 2.1 mm (see Figure 9), while the opposite side remains almost undistorted (see Figure 8). On the weld seam side, the maximum distortion (2.5 mm) occurs at the ends (see points A and B in Figure 8).

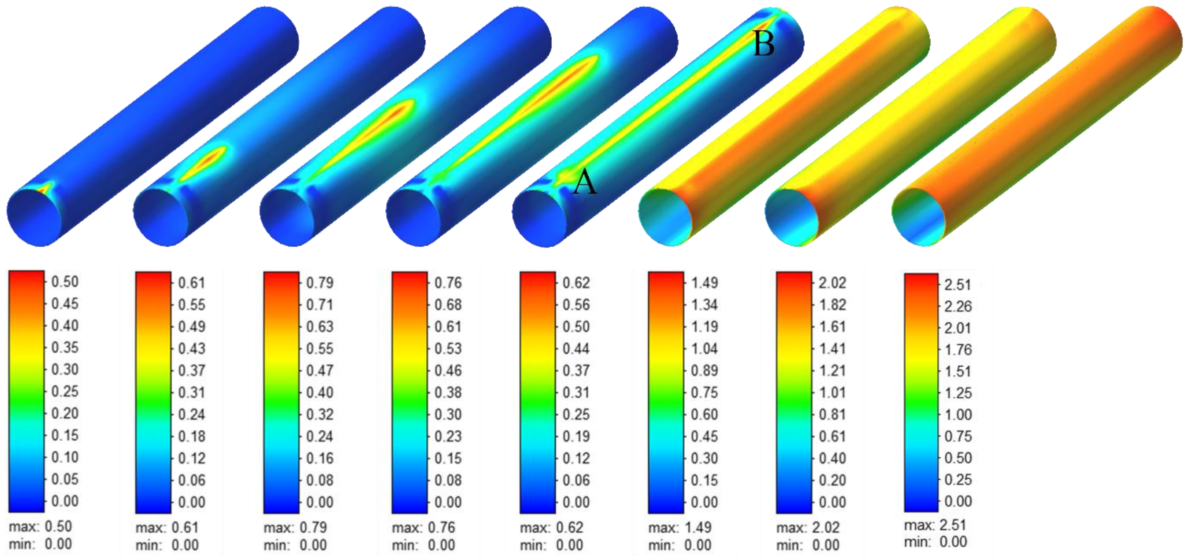

T = 5, 30, 60, 90, 120, 121, 150, 1920 sec (left to right)
Figure 8Distortion in pipe during welding (zero to 120 sec) and in cooling period (120 to 1920 sec).

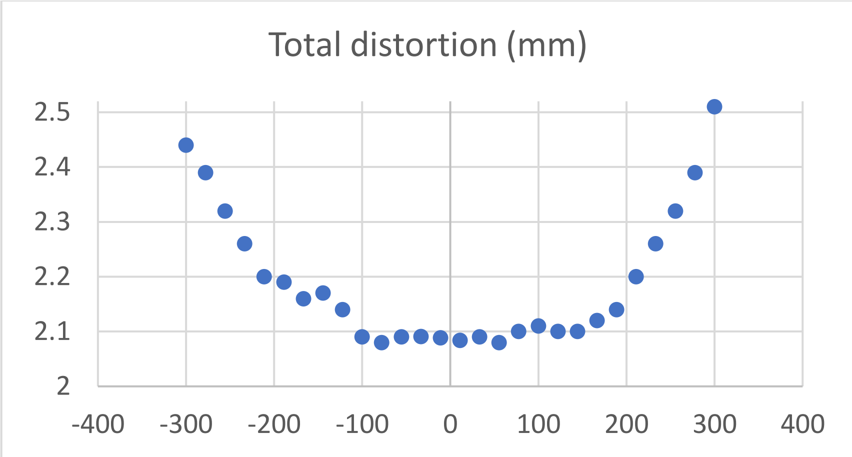

Figure 9 Distortion in the pipe at the end of the cooling period, after 1920 sec.

III. Conclusions

In this study, a fully coupled transient thermo-mechanical simulation technique was used to numerically replicate the welding behaviour on a seam welding with a nominal diameter of 80mm and a thickness of 1.5mm. The findings reveal that the residual stresses within and near the weld deposit are indeed influenced by the chosen welding sequence. An optimized selection of parameters can minimize distortion in the final welded part. The outcomes of the study are as follows –

1. The influence of optimized welding parameters is virtually simulated using finite element (FE) analysis.
2. In the HAZ, the highest temperature is localised and transient near the weld seam, ranging from 1773 to 737K, while temperatures away from the HAZ are below 350K only. Due to this temperature gradient, high residual stresses are generated.
3. In the entire weld seam, nearly uniform stress values of approximately 177 MPa are observed after cooling, which are lower than the yield value of the material.
4. The average value of distortion in the weld seam is 2.1 mm, while the maximum distortion of 2.5 mm occurs at the end.

References

[1] C. Liu, X. Zhou, L. Wang, J. Feng, Y. Li, and Y. Kang, "3D weld seam measurement in automotive manufacturing based on structured light reconstruction and deep learning segmentation," *Opt. Laser Technol.*, vol. 193, Jan. 2026, doi: 10.1016/j.optlastec.2025.114222.

[2] J. Yi, X. Kong, H. Tang, J. Zhang, Z. Chen, and L. Deng, "Weld seam extraction and path generation for robotic welding of steel structures based on 3D vision," *Autom. Constr.*, vol. 183, p. 106792, Mar. 2026, doi: 10.1016/j.autcon.2026.106792.

[3] S. K. Velaga, G. Rajput, S. Murugan, A. Ravisankar, and S. Venugopal, "Comparison of weld characteristics between longitudinal seam and circumferential butt weld joints of cylindrical components," *J. Manuf. Process.*, vol. 18, pp. 1–11, Apr. 2015, doi: 10.1016/j.jmapro.2014.11.002.

[4] A. Azka, "Preliminary assessment of surface inspection using visual imaging sensors for DEMO service weld seam," *Fusion Engineering and Design*, vol. 223, Feb. 2026, doi: 10.1016/j.fusengdes.2025.115553.

[5] Y. Lu, W. Kang, K. Liu, Z. Wang, and C. Guedes Soares, "Impact responses of aluminium stiffened plates near weld seams under quasi-static and dynamic loading," *Ocean Engineering*, vol. 349, p. 124207, Mar. 2026, doi: 10.1016/j.oceaneng.2026.124207.

[6] T. L. Teng, P. H. Chang, and W. C. Tseng, "Effect of welding sequences on residual stresses," *Comput. Struct.*, vol. 81, no. 5, pp. 273–286, Mar. 2003, doi: 10.1016/S0045-7949(02)00447-9.

[7] Y. Geng, H. Li, Y. Zhang, and X. Tian, "A novel 3D visual robotic servo approach for weld seam localization in multi-type complex intersecting joints," *Opt. Laser Technol.*, vol. 192, Dec. 2025, doi: 10.1016/j.optlastec.2025.114084.

[8] S. Song and P. Dong, "A framework for estimating residual stress profile in seam welded pipe and vessel components Part II: Outside of weld region," *International Journal of Pressure Vessels and Piping*, vol.

146, pp. 65–73, Oct. 2016, doi: 10.1016/j.ijpvp.2016.07.010.

[9] H. Liu *et al.*, "Efficient type identification and 3D positioning of weld seams for complex pre-weld conditions based on cross-structured light," *Measurement (Lond).*, vol. 260, Feb. 2026, doi: 10.1016/j.measurement.2025.119740.

[10] J. Zhang, X. Wang, Y. Sun, J. Li, and Y. Jiang, "Pitting behavior of austenitic stainless steel welded joints-A review," *Corrosion Communications*, Jan. 2026, doi: 10.1016/j.corcom.2025.04.007.

[11] Z. Zhu *et al.*, "Microstructure evolution and corrosion resistance of laser welded joints of high-nitrogen austenitic stainless steel under different atmosphere pressures and types," *J. Manuf. Process.*, vol. 156, pp. 727–744, Dec. 2025, doi: 10.1016/j.jmapro.2025.11.014.

[12] M. Hu, K. Wang, T. Li, D. Liu, K. Xu, and D. Li, "Microstructure and corrosion resistance of super duplex stainless steel 2507 joint by laser beam welding with argon-nitrogen mixed shielding gas," *Mater. Des.*, vol. 261, Jan. 2026, doi: 10.1016/j.matdes.2025.115413.

[13] T. Lan, T. Li, H. Liu, S. Tian, K. Liu, and Y. Wang, "Accurate localization and girth weld grinding planning for an in-pipe machining robot of thin-walled conical pipe," *Robot. Comput. Integr. Manuf.*, vol. 98, Apr. 2026, doi: 10.1016/j.rcim.2025.103124.

[14] W. Gong, H. Liu, Y. Zhao, and H. Zhang, "Research on the vibration fatigue of the socket welding in small branch pipes," *Nuclear Engineering and Design*, vol. 444, Dec. 2025, doi: 10.1016/j.nucengdes.2025.114356.

[15] Y. Ren, R. Skilton, I. Merrigan, and N. Mayfield, "Weldability of additive manufactured pipe features for fusion component replacement," *Nuclear Engineering and Technology*, vol. 58, no. 3, p. 104048, Mar. 2026, doi: 10.1016/j.net.2025.104048.

[16] A. Horváth, D. Kollár, and B. Kövesdi, "Distortions and residual stresses of NSS, HSS and hybrid box sections with single-bevel butt welds: An experimental study," *Thin-Walled Structures*, vol. 208, Mar. 2025, doi: 10.1016/j.tws.2024.112834.

[17] W. Wang *et al.*, "Microstructural regulation and crack suppression mechanisms of AlCoCrFeNiCux high entropy alloy coatings by resistance seam welding assisted electron beam cladding," *J. Alloys Compd.*, vol. 1036, Jul. 2025, doi: 10.1016/j.jallcom.2025.181840.

[18] W. Zhen, H. Li, and Q. Wang, "Simulation of residual stress in aluminum alloy welding seam based on computer numerical simulation," *Optik (Stuttg).*, vol. 258, May 2022, doi: 10.1016/j.ijleo.2022.168785.

[19] Y. Ai, S. Han, C. Lei, and J. Cheng, "The characteristics extraction of weld seam in the laser welding of dissimilar materials by different image segmentation methods," *Opt. Laser Technol.*, vol. 167, Dec. 2023, doi: 10.1016/j.optlastec.2023.109740.

[20] P. Li, F. Xu, J. Wang, H. Guo, M. Liu, and Z. Du, "DGConv: A Novel Convolutional Neural Network Approach for Weld Seam Depth Image Detection," *Computers, Materials and Continua*, vol. 78, no. 2, pp. 1755–1771, 2024, doi: 10.32604/cmc.2023.047057.

[21] S. Yu, Y. Guan, J. Hu, J. Hong, H. Zhu, and T. Zhang, "Unified seam tracking algorithm via three-point weld representation for autonomous robotic welding," *Eng. Appl. Artif. Intell.*, vol. 128, Feb. 2024, doi: 10.1016/j.engappai.2023.107535.

[22] J. Cai, Y. Wei, Z. Ouyang, X. Liu, H. Jin, and J. Chen, "Investigation on clockwise circular oscillating laser welding for the 5A06-H112 aluminum alloy: Energy distribution, seam appearance, microstructure, and mechanical properties," *Opt. Laser Technol.*, vol. 176, Sep. 2024, doi: 10.1016/j.optlastec.2024.111026.

[23] H. Liao *et al.*, "Effect mechanism of arc oscillation on microstructure and mechanical performance of SUS304 weld seams manufactured by local dry underwater double pulsed MIG welding," *Materials Science and Engineering: A*, vol. 887, Nov. 2023, doi: 10.1016/j.msea.2023.145752.

[24] J. Goldak, A. Chakravarti, and M. Bibby, "A new finite element model for welding heat sources," *Metallurgical Transactions B*, vol. 15, no. 2, pp. 299–305, Jun. 1984, doi: 10.1007/BF02667333/METRICS.

[25] Z. Jin, P. Dong, and S. Song, "An improved closed-form residual stress estimation method for girth welds in thin-walled pipe components," *Thin-Walled Structures*, vol. 213, Aug. 2025, doi: 10.1016/j.tws.2025.113343.

[26] Y. Liu, Z. Chen, P. Wang, H. Qian, X. Zhao, and N. Ma, "Mechanism analysis of welding distortion and residual stress induced by repair welding in thin-walled

pipes," *Ocean Engineering*, vol. 340, Nov. 2025, doi: 10.1016/j.oceaneng.2025.122253.

[27] U. Ehrnstén, P. L. Andresen, and Z. Que, "A review of stress corrosion cracking of austenitic stainless steels in PWR primary water," *Journal of Nuclear Materials*, vol. 588, p. 154815, Jan. 2024, doi: 10.1016/J.JNUCMAT.2023.154815.

[28] S. Ghosh, V. P. S. Rana, V. Kain, V. Mittal, and S. K. Baveja, "Role of residual stresses induced by industrial fabrication on stress corrosion cracking susceptibility of austenitic stainless steel," *Mater. Des.*, vol. 32, no. 7, pp. 3823–3831, Aug. 2011, doi: 10.1016/J.MATDES.2011.03.012.

[29] J. Chen, Y. Liu, Q. Chen, and Z. Xie, "Investigation of microstructure, mechanical performance, and corrosion resistance of thin-walled titanium welded pipe by annealing process," *Mater. Charact.*, vol. 218, Dec. 2024, doi: 10.1016/j.matchar.2024.114579.

[30] F. Hosseinzadeh *et al.*, "Residual stresses in austenitic thin-walled pipe girth welds: Manufacture and measurements," *International Journal of Pressure Vessels and Piping*, vol. 206, Dec. 2023, doi: 10.1016/j.ijpvp.2023.105016.

[31] Y. Liu, P. Wang, H. Fang, and N. Ma, "Mitigation of residual stress and deformation induced by TIG welding in thin-walled pipes through external constraint," *Journal of Materials Research and Technology*, vol. 15, pp. 4636–4651, Nov. 2021, doi: 10.1016/j.jmrt.2021.10.035.

[32] D. Deng and H. Murakawa, "Numerical simulation of temperature field and residual stress in multi-pass welds in stainless steel pipe and comparison with experimental measurements," *Comput. Mater. Sci.*, vol. 37, no. 3, pp. 269–277, Sep. 2006, doi: 10.1016/J.COMMATSCI.2005.07.007.

[33] S. J. Yan, S. K. Ong, and A. Y. C. Nee, "Optimal Pass Planning for Robotic Welding of Large-dimension Joints with Deep Grooves," *Procedia CIRP*, vol. 56, pp. 188–192, Jan. 2016, doi: 10.1016/J.PROCIR.2016.10.052.

[34] A. Pathak, S. Jaiswal, C. P. Singh, and G. K. Nhaichaniya, "Coupled thermomechanical FE analysis of multi-pass welding in thick pipe," *International Journal on Interactive Design and Manufacturing (IJIDeM) 2024 18:9*, vol. 18, no. 9, pp. 6825–6836, May 2024, doi: 10.1007/S12008-024-01857-4.